J Mater Sci (2008) 43:2058–2065
DOI 10.1007/s10853-007-2423-y

High temperature electrode reactions of Sr and Mg doped $LaGaO_3$ perovskite

Feng Zheng · Yu Chen

Received: 13 April 2007 / Accepted: 19 December 2007 / Published online: 31 January 2008

Abstract High-temperature phase reactions of Sr and Mg doped $LaGaO_3$ (LSGM) electrolyte with many electrode materials including Ag, Au, Pt, Sm doped CeO_2 (CSO), Sr doped $LaMnO_3$ (LSM), and Sm doped $SrCoO_3$ (SSCO) were investigated systematically by solid-state reaction and X-ray diffraction (XRD) analysis. Phase change and formation of minor phases were observed as a function of temperature. Single cells of LSGM electrolyte coupling with different electrode materials have been fabricated and tested by in situ ac impedance and IV curve measurement. The performance of single LSGM button cells was relative poor due to the occurrence of detrimental interfacial reactions.

Introduction

Assuming pseudo-cubic structure, Sr and Mg doped $LaGaO_3$ (LSGM) perovskites exhibit high oxide ion conduction and were considered as potential electrolyte materials for electrochemical devices, such as reduced or intermediate temperature solid oxide fuel cell (IT-SOFC) and oxygen pump etc. [1–6]. Although high power output being reported [7], issues of cost and phase stability (reactivity) with other cell components have to be considered prior to establish their due positions and realize full potential of application for those devices utilizing LSGM electrolytes.

F. Zheng (✉) · Y. Chen
School of Materials Science and Engineering, Central South University, Changsha, Hunan 410083, China
e-mail: fzheng@mail.csu.edu.cn

The composition of $(La_{1-x}Sr_x)_A(Ga_{1-y}Mg_y)_BO_3$ falls primarily in a single perovskite phase region with both x and y can vary from 0 to 0.2 moles and A/B ratio change from 0.98 to 1.02 [6]. In addition to the single phase, the formation of several minor phases that are undesirable for device application including $La_4Ga_2O_9$, $SrLaGaO_4$, and $SrLaGa_3O_7$ etc., may occur in the La_2O_3–SrO–Ga_2O_3–MgO quaternary system [6, 8]. Moreover, loss of Ga through vaporization at elevated temperature has been suggested thermodynamically and observed experimentally [6, 9–12]. Furthermore, sporadic studies of high-temperature phase reactions between LSGM and several well-known electrode materials were reported too [13–21]. For example, Huang et al. [13] showed that LSGM reacted with NiO at 1,350 °C for 4 h to form insulative phase $LaSrGa(Ni)O_{4-\delta}$ causing significant conductivity drop at low oxygen pressure. Hrovat et al. [14] revealed that LSGM reacted with $Ce_{0.8}Gd_{0.2}O_{1.9}$ to form insulative $SrLaGa_3O_7$ at 1,300 °C for 300 h by diffusion couple method. Conducting several close related studies, Zhang and colleagues [15–18] found that the LSGM-cell performance loss is attributed either to anodic Ni diffusion if sintering temperature is higher than 1,250 °C [15], or cathodic polarization due to elemental interdiffusion at prolonged testing [16]. In addition, $LaNiO_3$-based compound and $SrLaGa_3O_7$ have formed in NiO–LSGM and Sm-doped ceria (SDC)–LSGM binary powder mixtures after firing at 1,150–1,350 °C for 2 h, respectively. For the SDC–LSGM testing cell sintered at 1,350 °C, the ionic conductivity has dived more than 50% [17]. Moreover, several transition metals, such as Co, Ni, and Fe are readily reacting with LSGM in the order of Co > Ni > Fe when sintered at 1,150–1,350 °C for 2 h [18]. Although the interfacial resistance increasing with time, Horita et al. found a little evidence of interfacial phase formation between porous

$La_{0.6}Sr_{0.4}CoO_3$ (LSC) and LSGM with exception that there was some Co diffusion under current flow at 800 °C for 700 h [19]. Moreover, the activation energy for interface conductivity remained almost constant for different Sr concentration in LSC (137–142 kJ mol^{-1}) [20]. A pseudo-binary of $La_{0.9}Sr_{0.1}MnO_3$ (LSM)–LSGM has been investigated by Yi and Choi [21] by XRD. It appeared that there are three phase ranges existed in this mixture: single-phase cubic with LSM content less than 0.12; cubic plus hexagonal phases with LSM between 0.12 and 0.2; and hexagonal with orthorhombic phases for LSM between 0.2 and 1.0. It was hexagonal who dominants around 0.2–0.4, while orthorhombic's turn was between 0.7 and 1.0. In between (0.4 and 0.7) the mixture was hardly distinguishable due to peak overlapping. Four-probe dc measurement showed that the effect of LSM is harmful to cubic LSGM due to the increase in activation energy and the decrease in charge carrier concentration.

In order to have a rather complete and clear understanding of their properties, such as phase stability and electrochemical response, one objective of this work is to systematically investigate the high-temperature phase reactions between LSGM (as electrolyte) and many electrode materials including Ag, Au, Pt, Sm doped CeO_2 (CSO), Sr doped $LaMnO_3$ (LSM), and Sm doped $SrCoO_3$ (SSCO) by solid-state reaction and X-ray diffraction (XRD) analysis. Still another goal is to study the performance of single cells incorporating LSGM electrolyte and these electrode materials by in situ ac impedance and IV curve measurement.

Experimental procedures

Glycine-nitrate combustion process (GNP) [22–24] was employed to make the ceramic powders with desired stoichiometric composition of controllable doping content and oxygen vacancy concentration. The as-combustion powders were collected and calcined at an appropriate temperature to burn out residual organics and convert into desirable single perovskite or fluorite phase. The calcined powders of single phase were then attritor milled to eliminate agglomeration and achieve uniform size distribution. The fine powders of the desired perovskite or fluorite phase were then carefully weighed and an equal amount (in weight) of LSGM and each one of the electrode (Ag, Au, Pt, CSO, LSM, and SSCO) powders were mixed together and pelletized using a stainless steel die. The pellets were placed on top of an alumina plate for heat treatment in a box furnace. The furnace was equipped with a programmable ramping controller allowing precise temperature control. The samples were fired at high temperatures (ranging from 900 to 1,500 °C) using a ramping rate of 5 °C per min and held for 30 min to several hours (4 or 5 h at maximum) to achieve equilibrium (for solid-state phase reactions). Green density and "high temperature" density of the sample were monitored by measuring the change in weight and geometry of each pellet before and after heat treatment. X-ray analysis of mixed and crushed powders of the fired pellets was performed using a Siemens D-500 diffractometer. The diffraction spectrum of pure LSGM and each electrode powders was recorded and analyzed. These spectra are used as internal standards and references to monitor phase change and minor phase development of the mixture (electrolyte + electrode).

Thick sintered LSGM disks of various sizes (12–25 mm in diameter and 0.3–1 mm in thickness) were used as the electrolyte and coated by each electrode (by wet chemistry methods and diffusion bonding) to fabricate single button cells. Pastes of each electrode material made by colloid chemistry processing were applied to one side of the disk covering an area of 0.25–1 cm^2 and pre-fired at an appropriate temperature (850–950 °C for 30 min) to get a porous layer around 30–50 μm thick to serve as either the anode or cathode. Once the three functional cell layers (anode, cathode, and electrolyte) were physically bonded together, a thin layer of Pt paste was applied to the surface of both electrodes and fired at 900 °C for 30 min as electron collectors. An additional layer of Pt mesh was adhered to the Pt paste and fired at 900 °C for 30 min again to finish the fabrication of single cell assembly. These button cells were examined on an electrochemical testing system where the entire single cell assembly was then mounted on the top of an alumina tube attached in the middle of a special designed testing rig to form anode chamber as showed in Fig. 1.

Commercial compressed hydrogen (H_2) was adjusted through a set of regulators to give a mass flow rate of 50 mL per min and contained about 3 vol.% H_2O and went through a small alumina pipe inside the tube leading toward the anode chamber as fuel. The cathode chamber was open to air. Five Pt wires (two for anode, two for cathode, and one for reference electrode) were spot welded onto the Pt mesh to transfer electrons to an outside circuit for cell performance measurement (see Fig. 1). Ceramic sealant (Aremco 571 liquid and powders mixing in a weight ratio of 1:2) was used to seal the anode chamber while the cathode chamber was left open to air so plenty oxygen can migrate into reaction sites. The well-supported mini fuel cell (by alumina tube and testing rig) was then inserted into the hot zone of testing furnace where temperature was monitored by thermal couples attached to the vicinity of the cell. An appropriate heating profile was used to solidify the ceramic sealant at low temperatures and the in situ fuel cell testing was conducted afterwards when

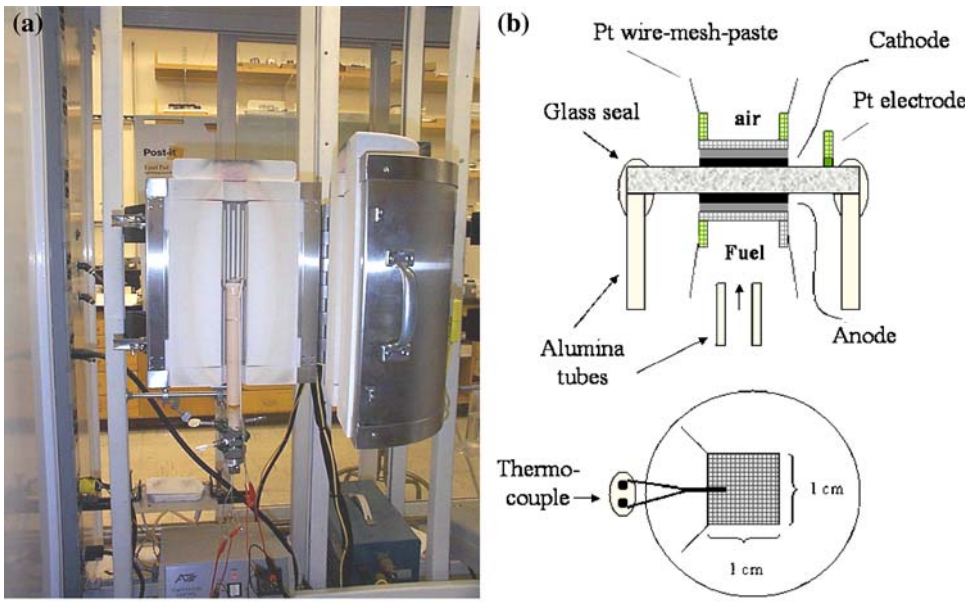

Fig. 1 Schematically draws of the button cell and testing rig

targeting the operating temperature and equilibrium condition was reached and achieved.

Results

Chemical compositions of $La_{0.9}Sr_{0.1}Ga_{0.8}Mg_{0.2}O_{2.85}$ (LSGM-1020), $La_{0.8}Sr_{0.2}MnO_3$ (LSM-20), $Sm_{0.5}Sr_{0.5}CoO_3$ (SSCO-50), and $(CeO_2)_{0.8}(SmO_{1.5})_{0.2}$ (CSO-20) were selected as the optimal SOFC materials and their powders were synthesized by glycine nitrate combustion process (GNP). The powders were calcined at suitable temperatures to get desirable single perovskite (LSGM, LSM, and SSCO) or fluorite (CSO) phase and followed by pelletization and sintering. The optimal heat treatment condition of sintering for each of these materials was 1,500 °C/4 h for LSGM-1020, 1,400 °C/4 h for LSM-20, and 1,100 °C/4 h for both SSCO-50 and CSO-20, respectively. The powders of single phase were then attritor milled for 3 h to obtain a uniform size distribution. The XRD spectra of these single phases were recorded and served as internal standards and references for further use.

Reaction couple of LSGM–LSM

Powders of equal weight of LSGM-1020 (monoclinic, similar to PDF 89-0080) and LSM-20 (monoclinic, similar to PDF 50-0308, peaks marked by stars*) were mixed together and palletized and fired at 1,100–1,400 °C at intervals of 100 °C for 5 h. The XRD spectrum of the mixture as a function of temperature with one on top of each other is presented in Fig. 2 with LSM-20 peaks marked with stars (*). Note these spectra have been normalized for better view where new peaks (differ from the bottom spectrum) appeared with intensity change occurred around 2θ of 30° are clear indication(s) of the formation and existence of secondary phase(s). The spectrum of the LSGM–LSM couple fired at 1,100 °C contains extra peaks corresponding mainly to Ga_2O_3 (PDF 41-1103), La_4SrO_7 (PDF 22-1430), and Mn_3O_4 (PDF 65-2776),

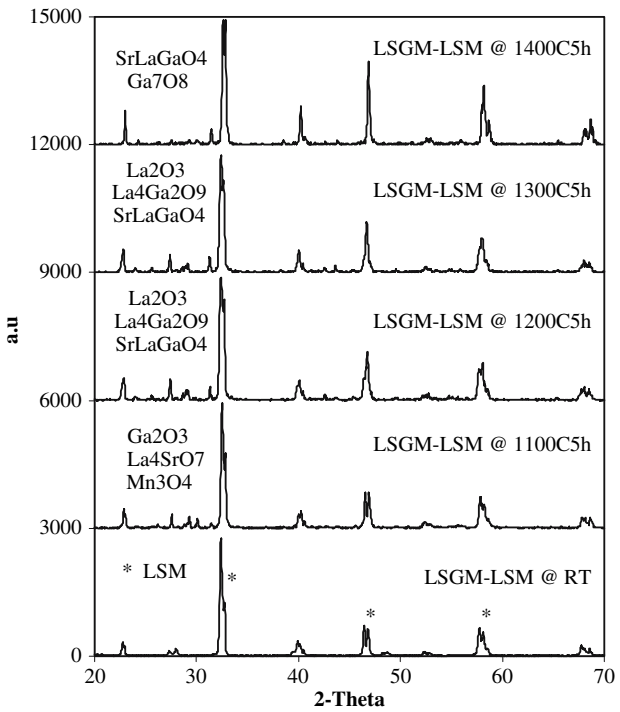

Fig. 2 XRD spectrum of LSGM–LSM reaction couple at different temperature

compared to the mixture (the spectrum at the bottom as reference). The spectrum at 1,200 and 1,300 °C look similar with each other where some of the extra peaks developed at 1,100 °C have changed into La_2O_3 (PDF 22-0369), $La_4Ga_2O_9$ (PDF 53-1108), and $SrLaGaO_4$ (PDF 24-1208). Those minor phases have further changed at 1,400 °C into $SrLaGaO_4$ (PDF 24-1208) and Ga_7O_8 (PDF 65-0117). Note here, none of these "high temperature" spectra looks exactly like the ones at room temperature despite the fact that their chemical compositions are identical and remain unchanged. Phase reactions have indeed occurred with increase of temperature.

Reaction couple of LSGM–SSCO

The XRD spectra of the mixture of both perovskite LSGM-1020 (monoclinic, similar to PDF 89-0080) with SSCO-50 (orthorhombic, PDF 53-0112, peaks marked by stars*) fired at different temperature are shown in Fig. 3. Note, secondary phases SrCoO (PDF 39-1084) and $SmSrGa_{0.7}O_3$ (PDF 50-1832) were developed (new peaks appeared with intensity change along the entire spectrum) at 1,100 °C. These newly formed minor phases begin to merge (corresponding peaks fade away) with the two parental main perovskite phases to form a sort of new single perovskite phase (similar to rhombohedral $La_{0.5}Sr_{0.5}CoO_{2.91}$, PDF 48-0122) plus minor phase $SmGaO_3$ (PDF 21-1060) around 1,200 °C. The appearance of this new single perovskite phase is well developed upon further heating up to 1,300 °C. Moreover, minor phases such as $SmSrGa_3O_7$ (PDF 50-1832) have being developed again around 1,400 °C (see peaks around 2θ of 30° for details). Note the spectrum at 1,300 °C is the cleanest one represented by the formation of the new rhombohedral perovskite $La_{0.5}Sr_{0.5}CoO_{2.91}$ phase whereas minor phases can exist below or above 1,300 °C here in the LSGM–SSCO reaction couple.

Reaction couple of LSGM–CSO

The XRD spectra of the mixture of perovskite LSGM-1020 (monoclinic, similar to PDF 89-0080) with fluorite CSO-20 (cubic, similar to PDF 65-5923, peaks marked by stars*) fired at different temperature are shown in Fig. 4. Note the structural difference here and the XRD features (peak distribution and shape) of these two phases are clearly distinguishable. In addition to minor phase (mainly Sm_2O_3, PDF 65-3183) development (started around 1,100 °C) the whole spectrum of the LSGM–CSO couple has changed considerably around 1,200–1,300 °C with all peaks (parental and minor phase) merged together where those corresponding to CSO barely disappeared. This is in contrast to the small and gradual peak (position and shape) change occurred below 1,200 °C. Further heating up to 1,400 °C leads to little change in the diffraction pattern where all the peaks are similar to those observable at

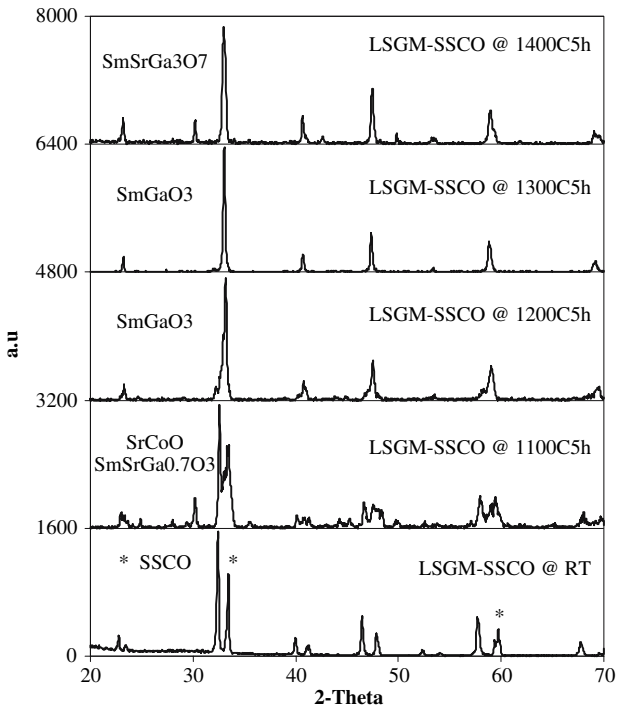

Fig. 3 XRD spectrum of LSGM–SSCO-50 reaction couple at different temperature

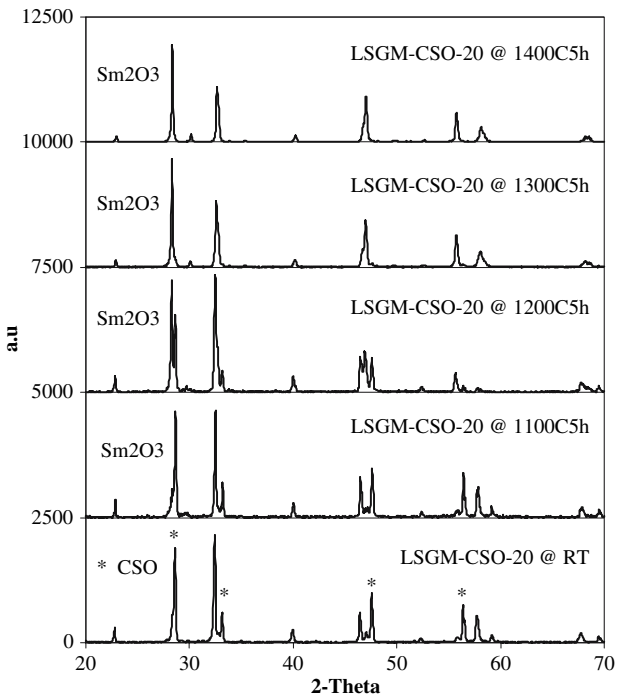

Fig. 4 XRD spectrum of LSGM–CSO reaction couple at different temperature

1,300 °C. Detailed analysis showed that the "high temperature" X-ray patterns are mainly consisted of one perovskite-like (LSGM, PDF 89-0080) plus one fluorite-like phase but they are not the simple combination or addition of their original two parental phases. In addition there is at least one minor phase (Sm_2O_3, PDF 65-3183) existing at high temperatures (see peaks around 2θ of 30°).

Reaction couples of LSGM with noble metals Ag, Au, and Pt

In addition to the above data presented in Figs. 2–4, we have also studied the reaction between LSGM with noble metals Ag (PDF 65-2871), Au (PDF 65-2870), and Pt (PDF 87-0646). At 900 °C, which is a typical processing temperature for such noble metals as either electrode or electron collector in fuel cell testing, LSGM reacts with Ag (with possible formation of Ag_2O_3, PDF 40-0909 and Ag_2Sr_3, PDF 65-3904, see Fig. 5) where no reaction could be detectable with Au (Fig. 6) or Pt (the middle spectrum in Fig. 7). However, electrochemical testing observation from symmetric cell Au|LSGM|Au and Pt|LSGM|Pt has showed phenomena indicating some sort of phase reactions occurrence under the influence of hydrogen and/or current flow. On the anode side (with H_2 flow) of the polished LSGM disk we can see clear diffusion marks and color change with both Au and Pt electrodes. Moreover, intergranular cracks observable by bare eyes were developed from anode side at Pt|LSGM|Pt cell. Furthermore, secondary phases such as $La_4Ga_2O_9$ (PDF 53-1108) and $GaPt_3$ (PDF 65-8000) were detected for the Pt|LSGM|Pt cell after it went through simulated SOFC operation and the result is shown in the top spectrum in Fig. 7. The normal practice for electrochemical cell testing starts from 500 to 900 °C at an interval of 50 °C and it takes about 30 min on average to collect the data at each temperature after the cell reached the equilibrium condition. The lowest testing temperature is limited by the conductivity of the electrolyte and for LSGM to have significant oxygen conduction and this would be somewhere around 500–550 °C. The highest testing temperature is chosen to have a direct comparison with the cell using thin YSZ electrolyte (typically up to 800 or 900 °C). The top two spectra are therefore comparable in term of heat treatment if we take all the testing time and temperature change into consideration. Clearly we can attribute the formation of the minor phases to the influence of H_2 flow as the extra peaks appear in the top spectrum while there are no such peaks in the middle spectrum (or the bottom spectrum also).

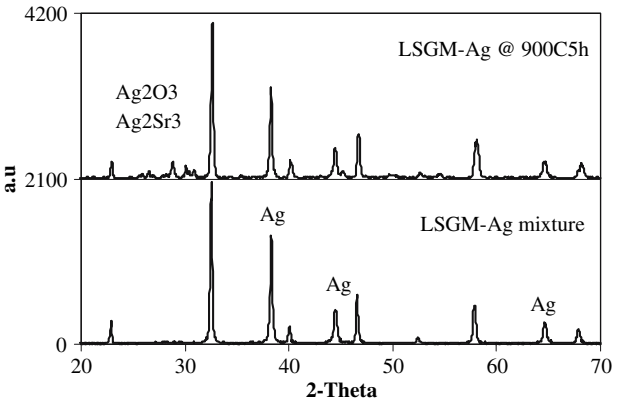

Fig. 5 Phase reaction between LSGM and Ag at 900 °C

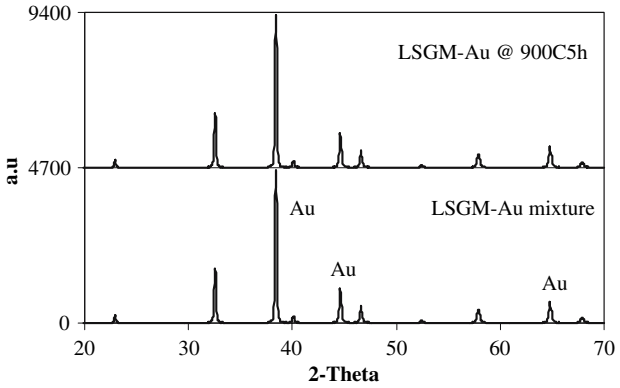

Fig. 6 Phase reaction between LSGM and Au at 900 °C

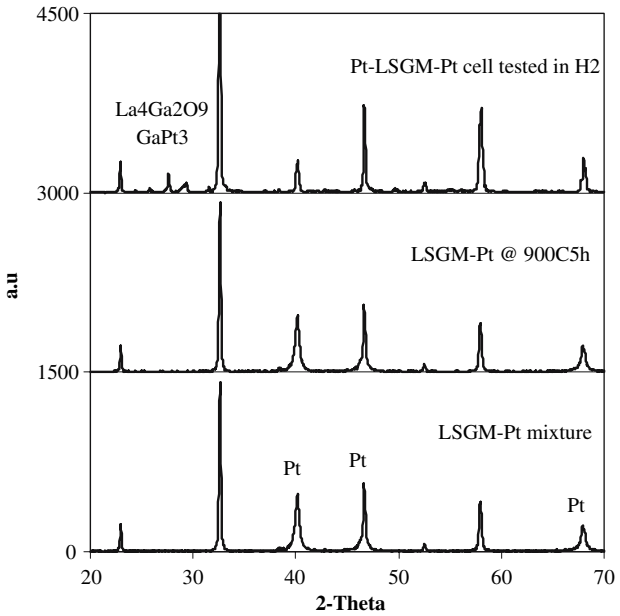

Fig. 7 The influence of H_2 on the phase reaction between LSGM–Pt

Density change

Furthermore, we have also monitored the density change by simply measuring the weight and dimensions of the

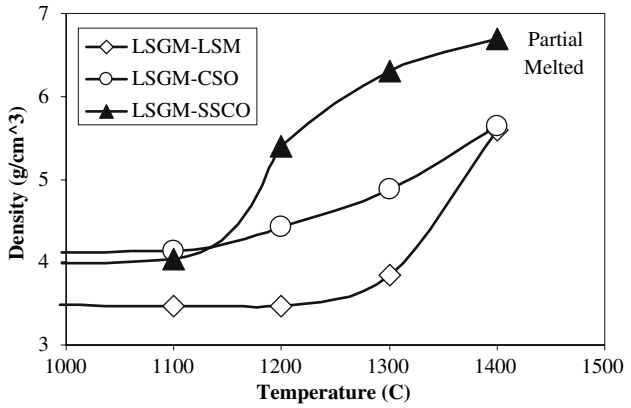

Fig. 8 Density change of LSGM reaction couples as a function of temperature

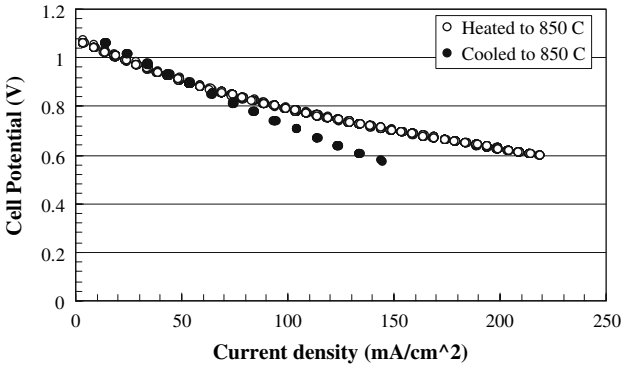

Fig. 9 IV curve of NiO–CSO–20|LSGM|SSCO-50 thick cell measured at heating (red, 850 °C) and cooling (blue, 850 °C after the cell was held at 900 °C overnight)

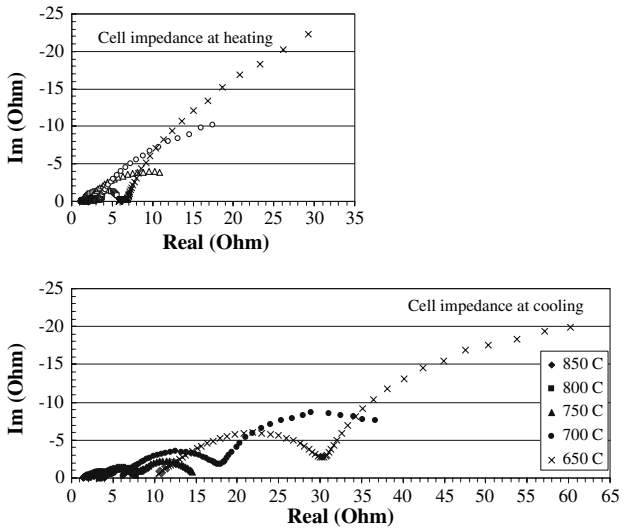

Fig. 10 AC impedance of NiO–CSO–20|LSGM|SSCO-50 thick cell measured at heating (top, 650–850 °C) and cooling (bottom, after the cell was held at 900 °C overnight)

sample before and after each heat treatment. There is no significant dimension change up to 1,100 °C for all samples and the density at that temperature is almost the same as the green density (shown as the flat lines on the left side in Fig. 8). The density of the LSGM–SSCO samples increases rapidly over 1,100 °C and reaches maximum somewhere between 1,300 and 1,400 °C, where the sample tested at 1,400 °C was partial melted and therefore no dimension measurement could be conducted. The density of the LSGM–CSO samples increases gradually over 1,100 °C and reaches a maximum at 1,400 °C here. The density of the LSGM–LSM samples almost does not change until 1,200 °C and increases quickly to a maximum at 1,400 °C. Recall the results from the phase reaction study (Figs. 2–7), the minor phases have already developed even before dimension change (at 1,100 °C) in these samples. This implies that it may be difficult to find the processing temperature–time window for electrode supported designs unless some of those minor phases are electrochemically beneficial or can at least be modified such that they are not detrimental to SOFC operation.

Single LSGM cells testing

AC impedance and IV curve measurement of thick LSGM-based single button cells for electrochemical testing conducted in the special designed testing booth showed in Fig. 1 have in general showed poorer-than-expected performances due to the abovementioned phase reactions between electrolyte and electrodes. One typical IV curve measured in positive hydrogen flow is given in Fig. 9 and the corresponding ac impedance data is plotted in Fig. 10. We can clear see how quick the performance of a thick button cell of NiO–CSO–20|LSGM|SSCO-50 (anode|electrolyte|cathode) has degraded overnight (area specific resistance increased from about 3–15 Ωohms). Note the data presented in the graph on the top was collected after the cell was heating up and reached to the designated testing temperature for at least 10 min to achieve equilibrium. The data in the bottom graph was collected on cooling after the cell being held at 900 °C overnight with other conditions being equal. Similar tendency with other electrodes for the LSGM button cells have been observed where there were roughly two to five times resistance increase overnight. Furthermore, we have noticed that the influence of fuel flow rate does have effect on cell performance in a short run but long-term effect remains insignificant.

Discussions

In addition to those facts already known to SOFC community, a systematic investigation conducted here may

permit us to find out some clear evidence of detrimental high temperature electrode reactions of LSGM (see Figs. 2–7) at prolonged operation condition. Generally speaking, most ceramic materials are likely to be electrical insulators. The product of interfacial reactions of any two ceramic materials is also insulator. Interfacial products can also be mechanically weaker than the parental materials despite the fact that most minor phases appearing in SOFC materials are thermodynamically stable [6, 8, 24, 25]. It has consequently long been considered a detrimental factor in SOFC development with regard to the appearance of these minor phases. They affect cell performance and therefore should be avoided.

The poor-than-expected cell performance (see Figs. 9 and 10) reflects all above mentioned electrode reactions and there is considerable work remaining to be done if we want to pursue LSGM thin film electrolyte fuel cells. Further notice that the reaction couple results from this study are consistent with those reported in literature where LSGM reacted with (1) a NiO-Sm doped CeO_2 anode at 1,150 °C after 2 h [17]; (2) Co_2O_3 at 1,150 °C after 2 h [17]; and (3) Fe_2O_3 at 1,350 °C after 2 h [18].

Conclusions

Based on high-temperature phase reaction study and single cell testing, we have found solid evidence that LSGM reacting with almost every electrode materials and quickly degrading its electrochemical cell performance. Although there is a desire to use LSGM as the materials choice of new electrolyte for IT-SOFC, the results presented here imply or indicate that LSGM electrolyte has considerable reactivity with many electrode materials and maybe not suitable for an electrode supported thin film fuel cell design. It will be very challenging for a LSGM-based thin film IT-SOFC to achieve high cell performance unless some novel methods are developed to retard or eliminate the interfacial reactions that have been observed with the electrode materials studied here.

Acknowledgements Partial work was conducted in Materials Sciences Division, Lawrence Berkeley National Laboratory, 1 Cyclotron Road, 62R0203, Berkeley, CA 94720, supported by the US Department of Energy under Contract no. DE-AC03-76SF00098. Special thanks are due to Dr. Steve Visco and Professor Lutgard DeJonghe for offering one of the authors (F. Zheng) the valuable opportunity and privilege to work in their labs.

References

1. Ishihara T, Matsuda H, Takita Y (1994) Doped $LaGaO_3$ perovskite type oxide as a new oxide ionic conductor. J Am Chem Soc 116:3801
2. Feng M, Goodenough JB (1994) A superior oxide-ion electrolyte. Eur J Solid State Inorg Chem 31:663
3. Huang PN, Petric A (1996) Superior oxygen ion conductivity of lanthanum gallate doped with strontium and magnesium. J Electrochem Soc 143:1644
4. Stevenson JW, Armstrong TR, Pederson LR, Weber WJ (1997) Processing and electrical properties of alkaline earth-doped lanthanum gallate. J Electrochem Soc 144:3613
5. Huang K, Tichy RS, Goodenough JB (1998) Superior perovskite oxide-ion conductor; strontium- and magnesium-doped $LaGaO_3$: I, phase relationships and electrical properties. J Am Ceram Soc 81:2565
6. Zheng F (2000) Phase stability and processing of the Sr and Mg doped lanthanum gallate. Ph.D. Dissertation, University of Washington
7. Inagaki T, Yoshida H, Sasaki T, Miura K, Adachi K, Hoshino K, Hosoi K, Ohara S, Fukui T, Ishihara T, High performance intermediate temperature solid oxide fuel cell with doped lanthanum gallate electrolyte, Ni–SDC cermet anode, and $Sm(Sr)CoO_3$ cathode. 2002 Fuel Cell Seminar, November 18–21, 2002, Palm Spring, California Palm Spring Convention Center, pp 423–425
8. Zheng F, Bordia RK, Pederson LR (2004) Phase constitution in Sr and Mg doped $LaGaO_3$ system. Mater Res Bull 39:145
9. Stevenson JW, Armstrong TR, Pederson LR, Li J, Lewinsohn CA, Baskaran S (1998) Effect of A-site cation nonstoichiometry on the properties of doped lanthanum gallate. Solid State Ionics 113–115:571
10. Yamaji K, Horita T, Ishikawa M, Sakai N, Yokokawa H (1999) Chemical stability of the $La_{0.9}Sr_{0.1}Ga_{0.8}Mg_{0.2}O_{2.85}$ electrolyte in a reducing atmosphere. Solid State Ionics 121:217
11. Yamaji K, Negishi H, Horita T, Sakai N, Yokokawa H (2000) Vaporization process of Ga from doped $LaGaO_3$ electrolytes in reducing atmospheres. Solid State Ionics 135:389
12. Kuncewicz-Kupczyk W, Kobertz D, Miller M, Chatillon C, Singheiser L, Hilpert K (2002) Vaporization studies of the La_2O_3–Ga_2O_3 system. J Am Ceram Soc 85:2299
13. Huang P, Horky A, Petric A (1999) Interfacial reaction between nickel oxide and lanthanum gallate during sintering and its effect on conductivity. J Am Ceram Soc 82:2402
14. Hrovat M, Ahmad-Khanlou A, Samardzȩija Z, Holc J (1999) Interactions between lanthanum gallate based solid electrolyte and ceria. Mater Res Bull 34:2027
15. Zhang X, Ohara S, Maric R, Mukai K, Fukui T, Yoshida H, Nishimura M, Inagaki T, Miura K (1999) Ni–SDC cermet anode for medium-temperature solid oxide fuel cell with lanthanum gallate electrolyte. J Power Sources 83:170
16. Inagaki T, Miura K, Yoshia H, Maric R, Ohara S, Zhang X, Mukai K, Fukui T (2000) High-performance electrodes for reduced temperature solid oxide fuel cells with doped lanthanum gallate electrolyte. II. $La(Sr)CoO_3$ cathode. J Power Sources 86:347
17. Zhang X, Ohara S, Maric R, Okawa H, Fukui T, Yoshida H, Inagaki T, Miura K (2000) Interface reactions in the NiO–SDC–LSGM system. Solid State Ionics, Diffus React 133:153
18. Zhang X, Ohara S, Okawa H, Maric R, Takehisa F (2001) Interactions of a $La_{0.9}Sr_{0.1}Ga_{0.8}Mg_{0.2}O_{3-d}$ electrolyte with Fe_2O_3, Co_2O_3 and NiO anode materials. Solid State Ionics 139:145
19. Horita T, Yamaji K, Sakai N, Yokokawa H, Weber A, Ivers-Tiffee E (2000) Stability at $La_{0.6}Sr_{0.4}CoO_3$ cathode/$La_{0.8}Sr_{0.2}Ga_{0.8}Mg_{0.2}O_{2.8}$ electrolyte interface under current flow for solid oxide fuel cells. Solid State Ionics 138:143
20. Horita T, Yamaji K, Sakai N, Yokokawa H, Weber A, Ivers-Tiffee E (2001) Electrode reaction of $La_{1-x}Sr_xCoO_{3-d}$ cathodes on $La_{0.8}Sr_{0.2}Ga_{0.8}Mg_{0.2}O_{3-y}$ electrolyte in solid oxide fuel cells. J Electrochem Soc 148:A456

21. Yi JY, Choi GM (2002) Phase characterization and electrical conductivity of $LaSr(GaMg)_{1-x}Mn_xO_3$ system. Solid State Ionics 148:557
22. Chick LA, Pederson LR, Maupin GD, Bates JL, Thomas LE, Exarhos GJ (1990) Glycine-nitrate combustion synthesis of oxide ceramic powders. Mater Lett 10:6
23. Chick LA, Maupin GD, Graff GL, Pederson LR, McCready DE, Bates JL (1992) Redox effects in self-sustaining combustion synthesis of oxide ceramic powders. Mater Res Soc Symp Proc 249:159
24. Zheng F (1996) Thermodynamics and phase behavior in lanthanum strontium manganites. MS Thesis, Washington State University
25. Zheng F, Pederson LR (1999) Phase behavior of the lanthanum strontium manganites. J Electrochem Soc 146(8):2810